Collective Dipole-Dominated Doping of Monolayer MoS2: Orientation and Magnitude Control via the Supramolecular Approach

Ye Wang, Sai Manoj Gali, Amine Slassi, David Beljonne, Paolo Samori

Collective dipole-dominated doping of monolayer MoS_2: orientation and magnitude control via the supramolecular approach

Ye Wang,[1] Sai Manoj Gali, [2] Amine Slassi,[2] David Beljonne,[2] Paolo Samorì[1*]

[1] Y. Wang, Prof. P. Samorì

University of Strasbourg, CNRS, ISIS UMR 7006, 8 Alleé Gaspard Monge, F-67000 Strasbourg, France.

E-mail: samori@unistra.fr

[2] Dr. S.M. Gali, Dr. A. Slassi, Prof. D. Beljonne

Laboratory for Chemistry of Novel Materials, Université de Mons, Place du Parc 20, 7000 Mons, Belgium.

Keywords: Two-dimensional material, MoS_2, doping, phthalocyanine, van der Waals heterostructures

ABSTRACT

Molecular doping is a powerful, tuneable and versatile method to modify the electronic properties of two-dimensional (2D) transition metal dichalcogenides (TMDCs). While electron transfer is an isotropic process, dipole-induced doping is a collective phenomenon in which the orientation of the molecular dipoles interfaced to the 2D material is known to be key to modulate and boost this electronic effect, despite it has not yet been demonstrated. Here we report a novel method towards the molecular functionalization of monolayer MoS_2 relying on the molecular self-assembly of metal phthalocyanine (MPc) and the orientation-controlled coordination chemistry of axial ligands. We have demonstrated that the subtle variation of position and type of functional groups exposed on the pyridinic ligand, yields a molecular dipole with programmed magnitude and orientation which is capable to strongly influence the opto-electronic properties of monolayer MoS_2. In particular, experimental results revealed that both p- and n-type doping can be achieved by modulating the charge carrier density up to $4.8\times10^{12}/cm^2$. Density functional theory calculations showed that the doping mechanism is primarily resulting from the effect of dipole-induced doping rather than charge transfer between MoS_2 and molecules. Our strategy to dope TMDCs is a highly modulable and robust, and it enables to enrich the functionality of 2D materials-based devices for high-performance applications in opto-electronics.

MAIN TEXT

Two-dimensional (2D) transition metal dichalcogenides (TMDs) have been the subject of intensive studies during the last decade because of their unique physico-chemical properties.[1] The most representative member of the family, MoS_2, is a semiconductor possessing a layer-dependent tunable bandgap (1.2 eV for bulk material and 1.9 eV for monolayer), high I_{on}/I_{off} ratio, large charge carrier mobility, and fast light response. Such unique features make MoS_2 a promising component for a variety of applications from (opto)electronics to valleytronics.[2] In particular, these properties open up a multitude of opportunities for the construction of high-performance ultra-thin heterojunction devices, e.g. p-n junctions and photodetectors.[3] Interestingly, the combination of organic molecules with TMDs was proven to be a versatile approach to tune the properties of the latter component via the 2D material's doping,[4] defect engineering,[5] device performance improvement,[6] etc..

Metal phthalocyanines (MPcs), an established family of symmetrical macrocycles comprising four iminoisoindoline units interacting with central metal ions, have been explored as molecular pigments for over a century. More recently, the applications of MPcs expanded to field-effect transistors, photovoltaic devices, phototherapies and catalysis by taking full advantage of the chemically modifiable structure which allows the tuning of many fundamental properties such as electron/hole conduction, light absorption and emission, etc.[7] The anionic aromatic ring tightly bonded with a cation center renders the conformationally planar MPcs highly stable against decomposition.[7b] Moreover, most MPcs form type II band alignment with monolayer

and few-layer MoS_2.[8] Thus, they are appropriate candidates to functionalize ultra-thin MoS_2 films, eventually via the formation of Van der Waals organic-inorganic heterostructures. This type of heterostructures has been proved to feature charge transfer from the LUMO of MPc to the conduction band of MoS_2, resulting in doping in field-effect transistors (FETs), [9] Raman enhancement,[10] photoresponse improvement,[11] etc.

The combination of MPcs and MoS_2 has been the subject of previous studies, all of them focused on either the charge transfer mechanism or the influence of the type of metal core on the energy of LUMO ($2e_g$ orbital) in the complex.[8-10, 12] Surprisingly, the exploration of axially functionalized MPcs has never been addressed. Coordination chemistry offers a broadest variety of functionalization solutions to decorate 2D materials beyond the two-dimensional space through the bonding of organic ligands to metal ions. Pyridine, being one among the most common ligands, enables a coordination involving the hybridization of its sp^2 electron lone pair to metal *d* orbitals, yielding a decrease of the 18-π aromaticity in MPcs, ultimately pulling the metal core out of the plane.[13] The axial pyridinic ligand is always standing perpendicular to the basal plane of the Pc ring. In fact, the four planar coordination sites in octahedral metal *d* orbitals are already occupied by four nitrogen atoms in the pyrrole rings, thus, the only possibilities for pyridine ligands to be coordinated are in the axial fifth and/or sixth sites. Previous works have shown that MPcs self-assemble on MoS_2 or graphite by forming supramolecular mono-molecular thick arrays with the Pc ring lying parallel to the basal plane of the substrate.[10, 14] In this regard, one can consider that once axial

ligands are coordinated onto self-assembled MPcs already coupled with MoS_2, they form ordered molecular arrays that are perpendicular to the MoS_2 /MPc heterojunction plane. When the axial ligands possess non-negligible dipole moments, these perpendicular molecular arrays could be translated as aligned molecular dipoles which are considered as a main factor to affect physical properties of MoS_2 in molecular doping.[4b] In this framework, it is essential to exploit the chemical programmability of axial ligands under the context of atomic-thin heterostructures.

In this work, we propose a radically novel strategy to molecular doping of monolayer MoS_2 by using MPcs as self-assembled template to grow ligands featuring relatively large molecular dipoles oriented perpendicularly the basal plane of the 2D material. Our approach consists of two-step functionalization: 1) Growth from solution of an ultra-thin self-assembled MPcs onto monolayer MoS_2; 2) Coordination of functionalized pyridines (fPys) onto the MoS_2/MPc heterostructures (Scheme 1**a**) in the vapor phase. In particular, we use two prototypical MPcs, i.e. zinc phthalocyanine (ZnPc) and cobalt phthalocyanine (CoPc) with distinct d-electron fillings (Co: d^7 and Zn: d^{10}). For fPy, we have chosen fluorine and amine substituted pyridines in different positions of the aromatic ring to ensure marked variation of the dipole moment magnitude and orientation, namely 3,5-difluoropyridine (3,5-FP), 3-fluoropyridine (3-FP), 2-fluoropyridine (2-FP) and 4-aminopyridine (4-AP). The chemical structures of MPcs and fPys are depicted in **Scheme 1a** and **1b**, respectively. Our approach holds three major advantages compared to the state-of-the-art: First, the low-temperature nature of the process of coordination of the central metal with the pyridine avoids occurrence of

re-aggregation of the MPcs thereby guaranteeing their planar packing onto monolayer MoS_2;[10] second, the use of a vapour phase deposition of the substituted pyridines means that the MPcs are not subjected to re-dissolution, thus guaranteeing the largest amount of fPy to be coordinated; third, the orientation of the ligand dipole in the fPy-MPc complex is ruled by geometric control of coordination bond, in full absence of π-π packing between fPy ligand and adjacent Pc rings which typically takes place in solution phase processes. In our textbook experiment, we found that simple variation of the magnitude and the orientation of ligand dipoles can be attained by changing the type and position of substitution groups in pyridine rings resulting in a tuneable modulation of charge carrier density in monolayer MoS_2/MPc heterostructures either via p- or n-doping. Both experimental and theoretical results provided unambiguous evidence for the pronounced effect of molecular dipole generated by axially bonded ligand, paving the way for controllable molecular doping of 2D materials.

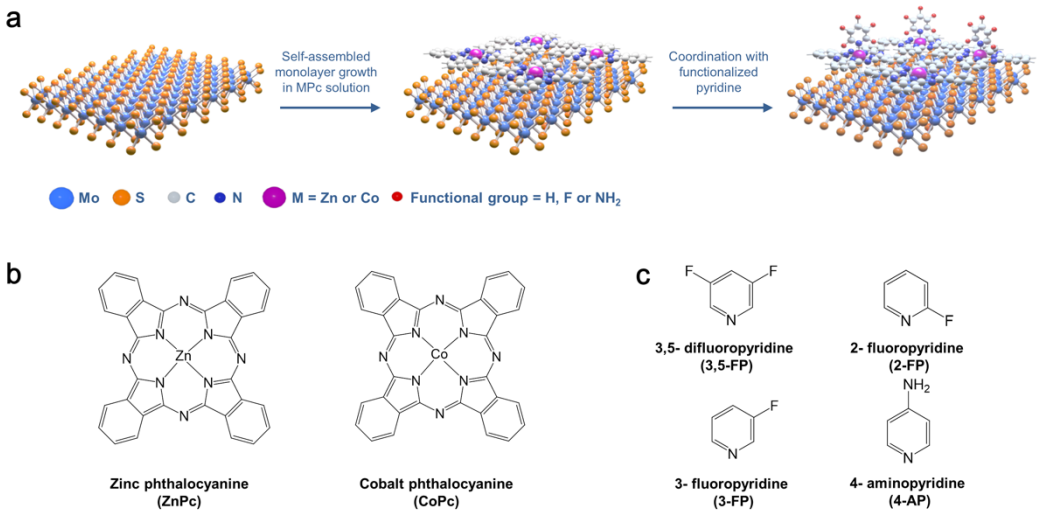

Scheme 1. (a) Illustration of two-step functionalization of ligand-coordinated MoS_2/MPc heterojunction. Chemical structure of **(b)** MPcs and **(c)** fPys used in this work.

To understand the electronic effect of axially functionalized MPc on MoS_2, we first gained qualitative insight into the effects of axial ligands on the monolayer MoS_2. **Figure 1a** and **b** show the AFM images of monolayer MoS_2 before and after the formation of 4-AP axial ligand on ZnPc. The pristine monolayer MoS_2 was found to be 0.73 nm thick, in agreement with the literature.[15] After the functionalization, the average height of the adlayer increased significantly thereby reaching 2.07 nm. Such an increase in thickness resulted from the physisorption of ZnPc, the binding of 4-AP and the out-of-plane displacement of zinc atom after coordination. The interfacial distance between ZnPc and MoS_2 was previously reported being ~ 0.37 nm,[16] the ZnPc monolayer thickness amounting to ca. 0.40 nm, the height of 4-AP being ca. 0.50 nm, and the displacement of Zn atom consisting of 0.05 nm.[13] We found that the difference of vertical distance before and after the functionalization amounts to 1.34 nm (**Figure 1d**), thus matching perfectly with the expected molecular configuration in **Scheme 1a**. High-resolution AFM images, as those displayed in **Figure 1c**, revealed that the morphology of self-assembled ZnPc/4-AP on MoS_2 consists of long parallel stripes with a width ranging between 12 and 20 nm. Such result is in line with previous STM observations with MPcs physisorbed onto MoS_2 forming stripes of closely packed two or more molecular rows with a gap between the stripes of 0.78 nm.[14b] The periodic structure also confirms that the coordination of ligands using our method does not destroy the self-assembled motif of ZnPc on MoS_2, enabling the edge-on packing of the pyridines. Raman spectroscopy also confirmed the successful functionalization of 4-AP ligand (**Figure 1e**). While a group of peaks appeared at high

wavenumber as a result of the formation of MoS_2/ZnPc heterostructure, corresponding to the vibration mode from Pc ring,[17] after the coordination of 4-AP, these features were preserved and combined with intensity enhancement at ~1405 cm^{-1} and 1510 cm^{-1}. The latter two peaks can be ascribed to the amino group and pyridine, respectively.[18] In all the combination of MPcs and fPys, we have observed similar signatures. XPS spectra of N 1s (e.g. see **Figure 1f**) also validated the efficient ligand functionalization. The proportion of nitrogen linked with metal increased from 36.95% (approx. 3 out of 8 nitrogen atoms) to 39.19% (approx. 3.6 out of 9 nitrogen atoms) after the coordination with 4-AP, indicating a 88.17% functionalization yield. The Mo 3d and S 2p spectra have demonstrated evident shifts according to different fPy functionalization, which could be found in **Figure S1**.

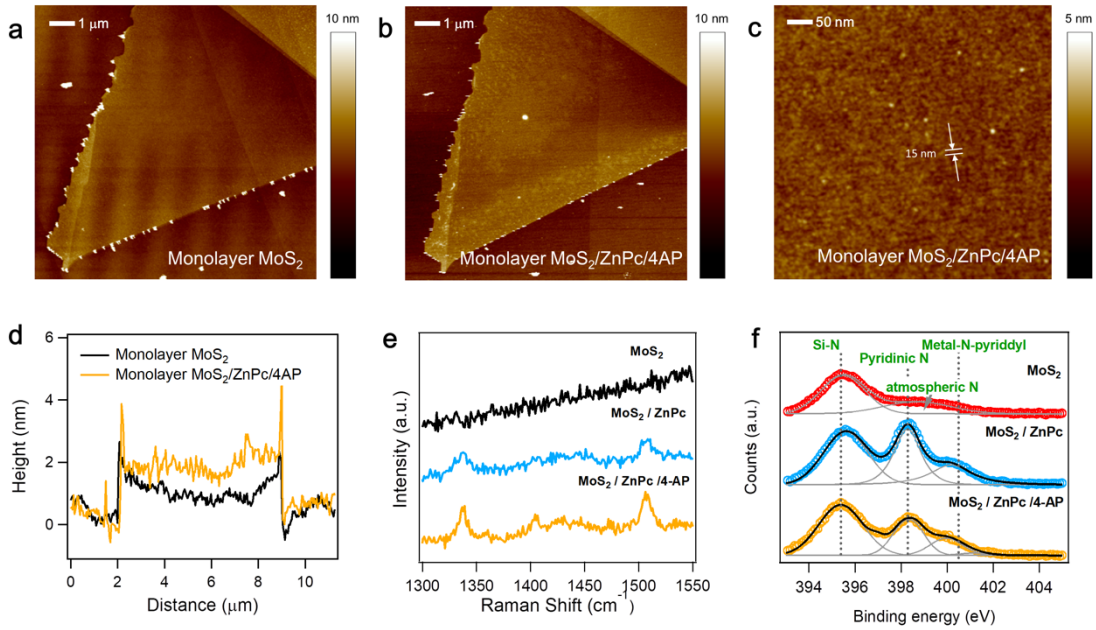

Figure 1. Topographic AFM image of **(a)** pristine monolayer MoS_2 and **(b)** monolayer MoS_2/ZnPc/4-AP, **(c)** the latter also on the sub-μm scale. **(d)** Height profile of monolayer MoS_2 and monolayer MoS_2/ZnPc/4-AP. **(e)** Raman spectra of monolayer MoS_2, monolayer MoS_2/ZnPc, and monolayer

MoS_2/ZnPc/4-AP in high wavenumber range. **(f)** XPS spectra of N 1s of monolayer MoS_2, monolayer MoS_2/ZnPc, and monolayer MoS_2/ZnPc/4-AP.

After confirming the effective functionalization, we explored how the axial ligands approach influences the electronic properties of MoS_2. We have fabricated back-gate, top-contact FETs with monolayer MoS_2 as channel material, as portrayed in **Figure 2a**. After the formation of self-assembled MPcs, we have observed a large shift of transfer curve (I_{ds}-V_g) to the positive direction (**Figure 2b** and **c**). Such evidence can be attributed to the formation of p-n junctions, in agreement with previous studies.[9, 11b] By further coordinating the fPys, we have observed shifts in two opposite directions: for 3,5-FP and 3-FP, the I_{ds}-V_g curves shift to positive voltages while for 2-FP and 4-AP, the curves shift to the negative direction.

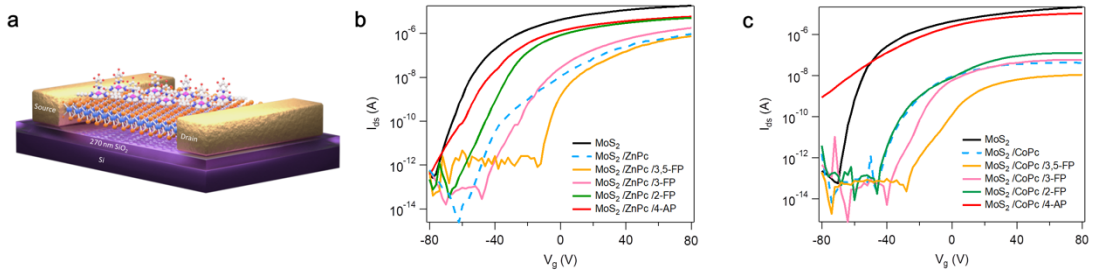

Figure 2. Electronic properties of ligand functionalized monolayer MoS_2. **(a)** Device structure of monolayer MoS_2 functionalized with MPc/fPy. **(b)** Comparison of transfer curves of MoS_2/ZnPc heterojuction coordinated with ligands. **(c)** Comparison of transfer curves of MoS_2/CoPc heterojuction coordinated with ligands.

The shift could be quantified by calculating the threshold voltage change (ΔV_{th}) in the transfer curve, as shown in **Figure 3a**. This value is known to correlate linearly with the charge carrier density change Δn by molecular doping in a semiconducting material, which could be solved with the following equation:

$$\Delta n = \frac{C_{ox}\,\Delta V_{th}}{e} = \frac{\varepsilon_{ox}\,\Delta V_{th}}{t_{ox}\,e} \qquad (1)$$

where Δn is the change in electron (negative charge) density, C_{ox} is the capacitance per unit area of 270 nm SiO_2, e is the elementary charge, and ε_{ox} is the dielectric constant of SiO_2, ΔV_{th} is the change of threshold voltage and t_{ox} is the thickness of SiO_2.

The calculated results are presented in **Figure 3b** in solid circles. We found that for MoS_2/ZnPc, ligand functionalization enables to modulate the carrier density in MoS_2 from -3.0×10^{12}/cm^2 in 3-FP to 1.8×10^{12}/cm^2 in 4-AP, while for MoS_2/CoPc, the modulation ranges from -3.5×10^{12}/cm^2 in 3-FP to 5.32×10^{11}/cm^2 in 4-AP, with respect to the reference case of MoS_2/MPc. The magnitude of the changes is surprisingly high, being comparable to the doping of ZnPc and CoPc on MoS_2 which amounts 1.8×10^{12}/cm^2 and 2.1×10^{12}/cm^2, respectively. Considering that the major charge carriers in MoS_2 are electrons, it is then obvious to conclude that 3,5-FP and 3-FP decrease in electron density in MoS_2/MPc, inducing p-doping, whereas 2-FP and 4-AP increase the electron density, inducing n-doping. The overall doping has also been observed to be dependent on the time of the fPys coordination. This time-dependent study also enables us to define the optimal functional time for each ligand to achieve the maximum doping effect on the MoS_2/MPc heterostructure. Detailed discussions are presented in **Figure S3** (Supporting Information). The tuneable either p- or n-type doping exhibits considerable changes in carrier densities in MoS_2/ZnPc which are comparable to effective molecular doping reported in the literature, being of the same orders of magnitude.[9, 19] The combination effect of ZnPc and 3,5-FP could decrease

the electron density by 3.5×10^{12}/cm^2, whereas the combination of CoPc and 4-AP could yield to an increase the electron density by 1.5×10^{12}/cm^2. The largest difference in electron density achieved with different binding ligands, namely 3,5-FP and 4-AP, reaches values as high as 4.8×10^{12}/cm^2 for ZnPc and 4.1×10^{12}/cm^2 for CoPc. These values are markedly larger than the values attained by using unsubstituted MPcs as dopants of monolayer MoS_2.[9, 11] Blank experiments carried out by interfacing fPys directly on MoS_2 via physisorption, in absence of the MPcs templating layer, revealed a much weaker effect after thermal annealing (at 95 °C for 3,5-FP, 3-FP, 2-FP and 200 °C for 4-AP) as a result of molecular desorption (**Figure S2**). Moreover, all fPys showed mild n-doping effect with V_{th} shift by 3 to 4 V ($\Delta n = 2.4\times10^{11}$/cm^2 to 3.2×10^{11}/cm^2), in stark contrast to our observations in the n- and p-type doping in the MoS_2/MPc/fPy hybrid heterostructure, especially when 3,5-FP and 3-FP are used as ligands. Thereby, the observed doping, which is strongly affected by the orientation of the dipoles, should be ascribed to the effect of the MPc-fPy coordination, in contrast to the random physisorption of fPys on MoS_2.

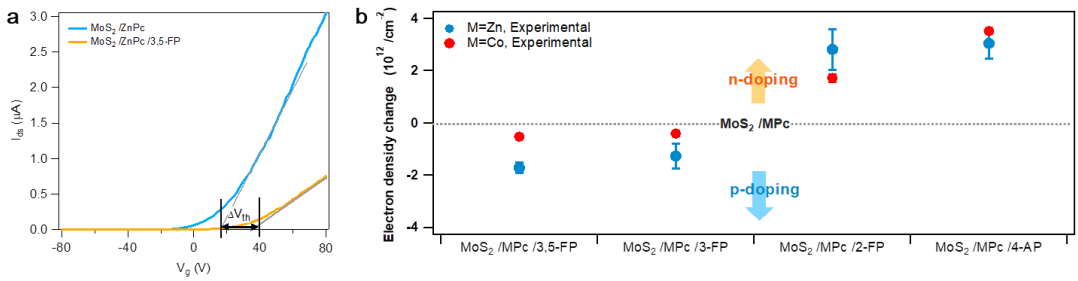

Figure 3. (a) Typical transfer curve of MoS_2/ZnPc and MoS_2/ZnPc/3,5-FP showing the calculation of ΔV_{th} before and after ligand functionalization. (b) Charge carrier density shift in monolayer MoS_2 after ligand functionalization of fPys on MPc obtained from FET measurements with comparison to the theoretical results calculated from work function analysis.

In order to investigate the role of ligand functionalized MPcs in modulating the charge carrier density, we have carried out density functional theory (DFT) calculations. It is indeed notorious that the component of molecular electric dipoles perpendicular to the surface of 2D materials exert a polarization capable of shifting the surface work function, hence inducing a local doping.[20] Accordingly, we have calculated the theoretical work function (φ_{th}) of MoS_2/MPc/fPy heterostructures in conjunction to the axial dipole moment of these heterostructures and the dipole induced electrostatic potential of isolated molecules at vacuum level (E_p) in order to trace the relative changes in φ_{th} of MPc/fPys. All MPc/fPys form type II heterostructures with MoS_2, irrespective of the type of axial ligands, as emphasized in previous works, [16,17] wherein the HOMO of MPc/fPys is located within the band gap of MoS_2 monolayer (see **Figures S4-S6**). Theoretical values for the work function (φ_{th}) of MoS_2/ZnPc and MoS_2/CoPc are found to be 5.13 eV and 5.18 eV respectively, in close agreement with the experimental observations (see **Figure 4** and **Table 1**). Upon addition of the axial 'un-functionalized' pyridine (Py) ligand to MPc, the work function was found to increase. This is because MoS_2/MPc/Py features an axial dipole moment (perpendicular to and directed towards the basal plane of MoS_2 surface, note as dipole 1) originating from the ligand induced metal-N coordination bonding. When the axial pyridine ligand has functional groups on the aromatic ring, additional changes in the work function can be predicted: MoS_2/MPc/3,5-FP and MoS_2/MPc/3-FP showed relatively higher φ_{th} values than MoS_2/MPc/Py, whereas MoS_2/MPc/2-FP and MoS_2/MPc/4-AP displayed comparatively lower φ_{th} values. These relative changes in work function of

MoS_2/MPc/fPys with respect to MoS_2/MPc/Py follow the variation in the net dipole moment (axial component, note as dipole 2) of the functionalized molecules. To comprehend the relative variation in net dipole moment due to pyridine functionalization and its subsequent impact on the observed work function changes, we define dipole 2 as the difference between the net dipole moments of functionalized pyridine molecules (MoS_2/MPc/fPys) and dipole 1, which is the net dipole moment of un-functionalized pyridine (MoS_2/MPc/Py). Dipole 2 therefore quantifies the contribution of functional groups present on the pyridine ligand to the net dipole moment of MoS_2/MPc/fPys, wherein a positive (negative) value of dipole 2 partially cancels (add to) the contribution of dipole 1. The net dipole moments of MoS_2/MPc/3,5-FP and MoS_2/MPc/3-FP are lower than that of MoS_2/MPc/Py, as the relative positioning of fluorine atoms in 3,5-FP and 3-FP generates a dipole electric field that is directed away from the MoS_2 surface (positive dipole 2), thereby partially cancelling the field induced by the metal-N coordination. In contrast, the net dipole moments of MoS_2/MPc/2-FP and MoS_2/MPc/4-AP were found being higher compared to MoS_2/MPc/Py, because the normal component of the dipole carried by the functional groups adds in phase to the metal-N coordination dipole, both being directed towards the surface (see **Figure S7**). Furthermore, as presented in **Figure 4**, the variation in the dipole moment of MoS_2/MPc/fPy heterostructures and the associated work function changes are proportional to the dipole induced electrostatic potential of isolated molecules at their vacuum level (E_p). Because of the atomic thickness of monolayer MoS_2, the electric field generated by aligned molecular dipole could result in a large

charge carrier modulation and thus promote doping, analogously to a local electric gate.[4a] Hence, with reference to MoS_2/MPc/Py, a relative p-doping could be predicted for MoS_2/MPc/3,5-FP and MoS_2/MPc/3-FP that showed a reduced normal dipole moment, while a relative n-doping would be expected for MoS_2/MPc/2-FP and MoS_2/MPc/4-AP yielding an increased dipole moment. Photoelectron spectroscopy measurements in air (PEYA) in **Figure S8** confirmed that experimentally, the work function values shift with the same trends observed in DFT calculations, with 4-AP reducing the work function value to 5.11 eV and 3,5-FP increasing the work function up to 5.30 eV. The great modulation of work function revealed that the Fermi level of monolayer MoS_2 is largely influenced by the ligand functionalization with much more important contribution coming from the molecular dipole.

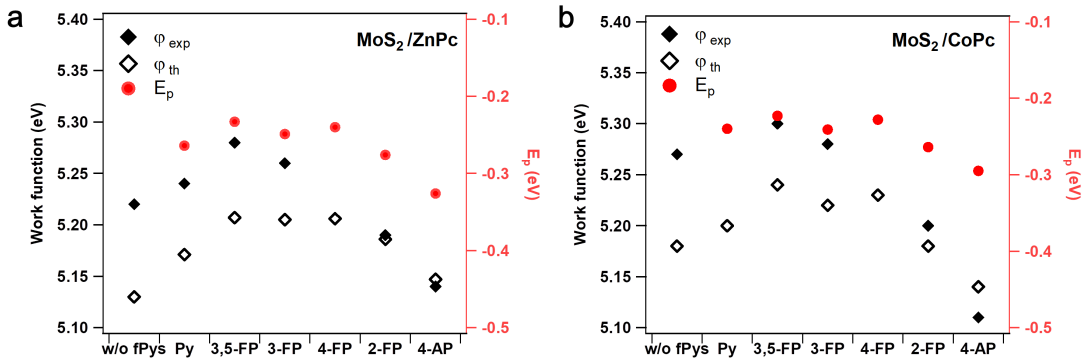

Figure 4. Calculated work function of MoS_2/MPc/fPys for **(a)** M=Zn, and **(b)** M=Co. The φ_{exp} stands for experimental work function values measured by PhotoElectron Yield counter operating in Ambient conditions (PEYA) which are presented in Figure S8. The work function trends follow the computed dipole induced electrostatic potential (E_p) of the isolated molecules at vacuum level.

Molecule	φ_{exp} (eV)	φ_{th} (eV)	D_{total} (D)	E_p (eV)
MoS_2/ZnPc/fPys				
MoS_2/ZnPc	5.22	5.130	-1.333	-0.136
MoS_2/ZnPc/Py	5.24	5.171	-7.465	-0.264

MoS_2/ZnPc/3,5-FP	5.28	5.207	-5.431	-0.233
MoS_2/ZnPc/3-FP	5.26	5.205	-6.455	-0.249
MoS_2/ZnPc/4-FP	--	5.206	-5.767	-0.240
MoS_2/ZnPc/2-FP	5.19	5.186	-7.924	-0.276
MoS_2/ZnPc/4-AP	5.14	5.147	-10.661	-0.326
MoS_2/CoPc/fPys				
MoS_2/CoPc	5.27	5.18	-1.522	-0.129
MoS_2/CoPc/Py	--	5.20	-6.679	0.240
MoS_2/CoPc/3,5-FP	5.30	5.24	-4.957	-0.223
MoS_2/CoPc/3-FP	5.28	5.22	-6.006	-0.241
MoS_2/CoPc/4-FP	--	5.23	-5.109	-0.228
MoS_2/CoPc/2-FP	5.20	5.18	-7.218	-0.264
MoS_2/CoPc/4-AP	5.11	5.14	-9.985	-0.295

Table 1. Work function and dipole moment of MoS_2/MPc/fPy systems. φ_{th}: work function of MoS_2 monolayer functionalized with MPc/fPys. φ_{exp}: work function values measured by PhotoElectron Yield counter operating in Ambient conditions (PEYA) which are presented in Figure S8. D_{total}: total dipole moment of MoS_2/MPc/fPy in Debye, negative sign indicates dipole moment directed towards basal plane of MoS_2 surface. E_P: Dipole induced electrostatic potential (in eV) of isolated ligand at vacuum level. Additional calculations were performed on MoS_2/MPc/4-fluoropyridine (4-FP) for consistency in φ - Dipole moment trends.

Not only the electrical properties in MoS_2 are strongly influenced by ligand-induced dipoles, but also the optical properties are greatly affected. The direct bandgap at K point enables strong photoluminescence (PL) emission in monolayer MoS_2. Typical PL spectra of monolayer MoS_2 can be found in **Figure 5a**. We could find two major peaks originated from spin-orbit splitting of transition metal, one at lower energy, denoting A exciton peak, and the other, the B exciton peak, at higher energy. Referring to the literature,[21] A exciton peak could be split into two components after Lorentzian fitting, which are noted as X^- at around 1.83 eV, and X at around 1.87 eV. The ability of binding an extra electron to neutral exciton X (one electron binds with one hole) gives rise to the negative trion X^- with binding energy of around 40 meV in room temperature, when the charge carrier density in

monolayer MoS_2 is in excess of electrons. Hence, the switching of intensity of trion and exciton mirrors the balance between electrons and hole in MoS_2 sheets, in other words, the doping level in MoS_2. We are able to quantify the trion weight γ by

$$\gamma = \frac{I_{X^-}}{I_{total}} = \frac{I_{X^-}}{I_{X^-}+I_X} \quad (7)$$

As is demonstrated in the left panel in **Figure 5a**, the electronic coupling of ZnPc on MoS_2 caused decrease in trion from 0.71 to 0.31, implying compensating of excessive negative charges in pristine MoS_2, inducing p-dope decreasing the electron. After coordinating fPys, 3,5-FP and 3-FP yielded a further decrease of trion weight (middle panel in **Figure 5a**), whereas 2-FP and 4-AP brought back the recombination of trion (right panel in **Figure 5a**). The quantified values of trion weight are plotted in **Figure 5b**. Unfunctionalized pyridine whose dipole moment induced by the functional groups is considered to be 0 showed trion weight between 3-FP and 2-FP after coordinating with ZnPc, indicating that the inversion of sign of dipole 2 could alternatively influence the regulation of trion weight. Similarly, in **Figure 5c** and **d**, despite the severe suppression of the formation of trions after doping with CoPc, the coordination of fPys led to a similar trend observed for ZnPc, but in a smaller value range.

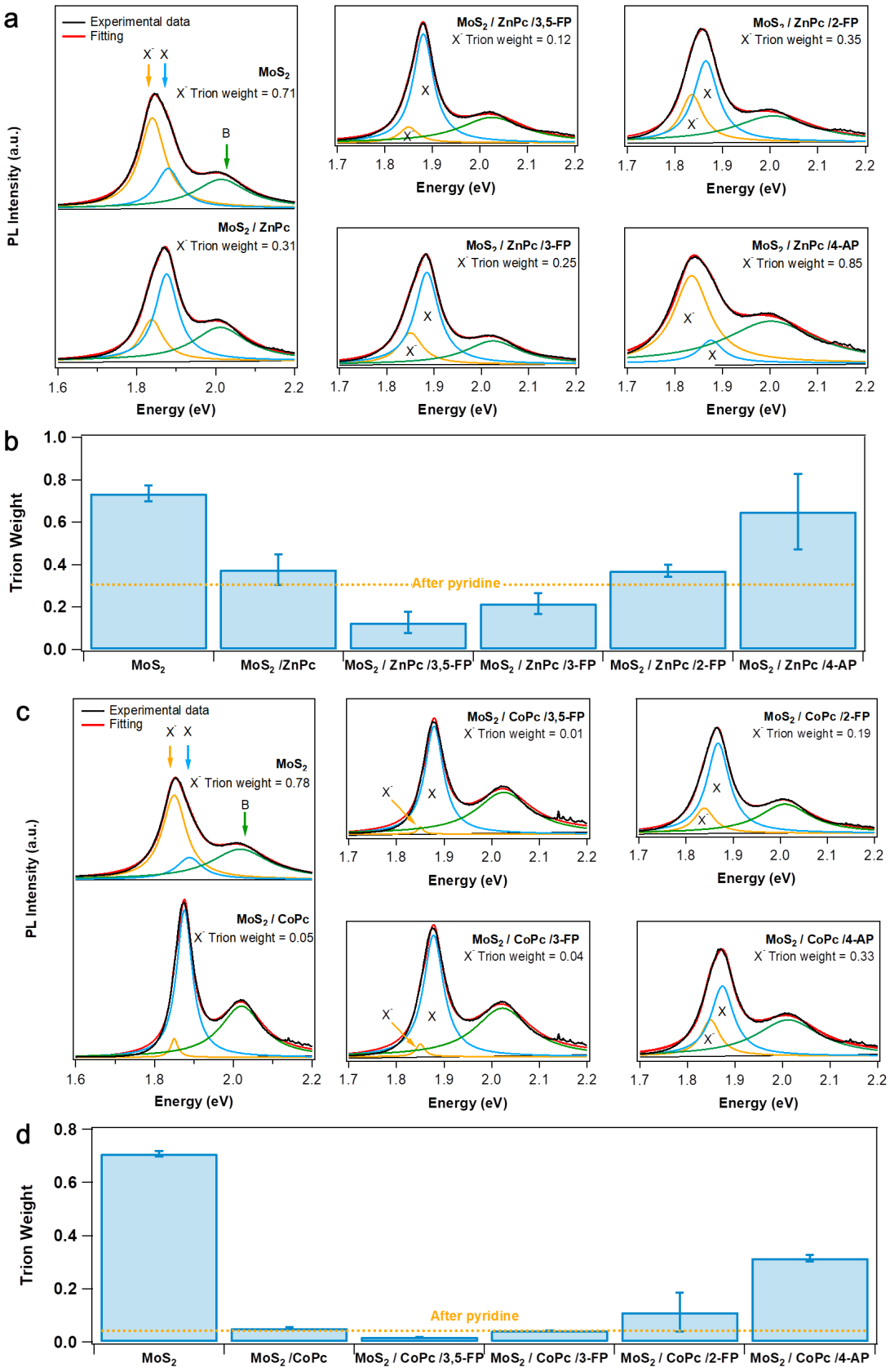

Figure 5. Photoluminescence spectra of **(a)** MoS_2/ZnPc and **(c)** MoS_2/CoPc coordinated with fPys. **(b)** and **(d)** average trion weight of each ligand coordinated heterojunction with ZnPc and CoPc, respectively.

To exclude the doping originated from physisorption of pyridines and solvents, we performed control experiments without MPcs with the same experimental procedures whose results are portrayed in **Figure S9**. In particular, similar results were found when doing blank tests with MoS_2 based FETs coated by fPys, in absence of templating MPcs. Upon thermal annealing treatments, the fPhys were found to desorb leading to negligible doping effects of the MoS_2. The only small amount of fPys remained on the surface possess a random geometrical configuration without alignment of molecular dipoles, thus eliminating the molecular gating effect induced by a collective process. The trion weight can be translated to charge carrier density by means of the mass action model. We found approximate values as in FET analysis (shown in **Table S1**), confirming that molecular dipole induced doping by fPys is very little affected by the optical properties of MPcs.

Furthermore, Raman vibrations of monolayer MoS_2 were also found to be sensitive to the coordination of fPys. Two main Raman modes of undoped MoS_2 were measured, i.e. the out-of-plane E^1_{2g} mode at ~386 cm^{-1} and the in-plane A_{1g} mode at 405 cm^{-1}. Compared to the bare MoS_2, the addition of MPc resulted in small blueshift in A_{1g} peak and nearly no change in E^1_{2g} peak (**Figure S10**). It is reported in the literature that doping could affect the A_{1g} mode in higher extent than E^1_{2g} mode, thus yielding shifts in peak position. The redshift corresponds to the increase in electron concentration which softens the Raman vibration, and the blueshift corresponds to decrease of electron concentration which hardens the vibration.[19] The ligands, accordingly, led to non-negligible shift in A_{1g} modes. As shown in **Figure 6a**, 3,5-FP and 3-FP blueshifted the A_{1g} peak for 0.402 cm^{-1} and 0.120 cm^{-1} respectively, indicating p-doping. 2-FP and 4-AP induce redshift of 0.213 cm^{-1} and

0.564 cm^{-1}, reflecting n-doping. The observed effect is in perfect agreement with FET analysis, DFT calculation and PL measurements providing an unambiguous evidence that MPcs p-dopes the pristine MoS_2. The average Raman shift of A_{1g} peak between different fPy ligands could be as much as 0.966 cm^{-1}, while the E_{2g} peak remained constant under the influence of molecular dipoles. (**Figure 6b**). The full width at half maximum (FWHM) of A_{1g} peak was also found to be broadened by n-doping and sharpened by p-doping, demonstrated in **Figure 6b**. This could be explained by enhanced electron-phonon coupling of A_{1g} mode by increasing the electron density in MoS_2. The variation of FWHM could attain ~1 cm^{-1} by changing the functionalized ligand.

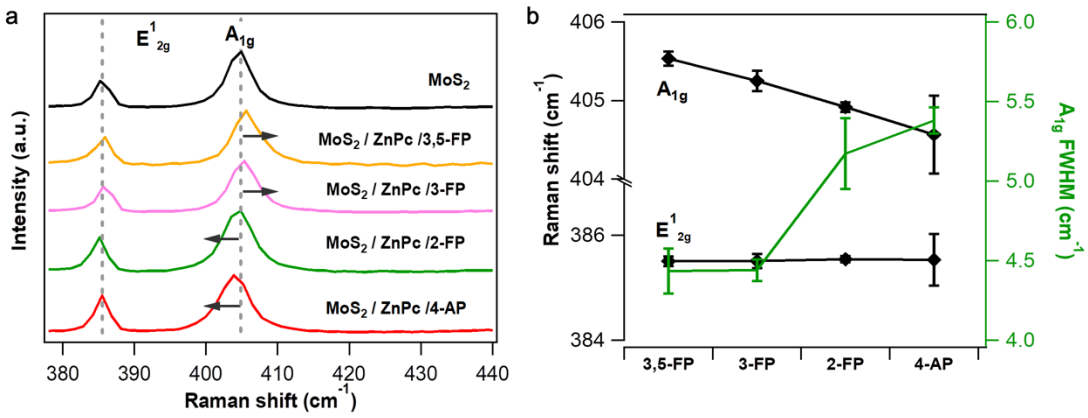

Figure 6. (a) Raman spectra of pristine MoS_2 and functionalized with ZnPc/fPys. **(b)** Plot of the shift in E^1_{2g} mode and A_{1g} mode, and the variation of full width of half maximum (FWHM) of A_{1g} peak upon the functionalization by different fPy ligands.

CONCLUSIONS

In summary, we have demonstrated a new strategy for doping 2D semiconductors by combining supramolecular self-assembly at surfaces, coordination chemistry and molecularly driven electrical gating. Aligned molecular dipoles having a precise

orientation with respect to the basal plane of the MoS_2 surface were generated by taking advantage of the versatile functionalization of pyridine molecules and the geometry-controlled ligand binding direction in zinc and cobalt phthalocyanines. Electrical analysis, spectroscopic measurements and DFT calculations confirmed that not only charge transfer between axially functionalized MPc and monolayer MoS_2 participate in the tuning of properties, but also that the aligned dipole moments generated by pyridinic ligands play a much more important role in controlling the either n- or p-type doping of MoS_2 by modulating the charge carrier density up to $4.8 \times 10^{12}/cm^2$. Optical properties, such as exciton/trion switching and Raman features were found to be largely influenced by the molecular dipoles. Our results revealed how the variation of molecular dipole could strongly affect both the electrical and optical properties of underneath substrate material. A brand-new concept in realizing the controllable doping by organic molecules without the need of cumbersome synthesis or functionalization with complex chemical reactions has been proposed. The large magnitude of this doping effect is guaranteed by the collective nature of the dipole effect induced by the simultaneous alignment of a huge number of molecules yielding a nonlocal macroscopic effect. Our approach of molecularly tuned dipole induced doping is highly modulable and generally applicable to other 2D materials, thereby opening new avenues for enhancing the performances of 2D materials for applications in opto-electronics.

EXPERIMENTAL SECTION

Sample preparation. Monolayer MoS_2 were mechanically exfoliated from commercially available molybdenite crystals (Furuchi, Japan) using the scotch tape method and transferred on thermally oxidized heavily *n*-doped silicon substrates (Fraunhofer Institute IPMS, $\rho_{Si} \sim 0.001$ Ω·cm, $t_{ox} = 270$ nm). Their thickness was monitored by optical microscope combined with Raman spectroscopy and Atomic Force Microscopy (AFM). The samples were thermally annealed at 200 °C inside a vacuum chamber to desorb atmospheric adsorbates. ZnPc and CoPc are purchased from Merck. The MoS_2/MPc hybrids were realized by immersing monolayer MoS_2 into 0.5 mM MPc in anhydrous solution, then rinsed vastly and thermally annealed in nitrogen to remove aggregates and evaporate solvents. To avoid the desorption of MPc on MoS_2 when reacting with ligands in solvent environment, the coordination of pyridinic ligand (TCI Chemicals) is reacted in vapor phase where 50 μL of pure pyridine was added in a 60 mL closed beaker containing the MoS_2/MPc heterostructure on Si/SiO_2 chip. The whole beaker is heated up to an ad hoc temperature (85 °C for 3,5-FP, 3-FP, 2-FP and 175 °C for 4-AP) to form pyridine vapours to enable the contact with MPc. The optimal functionalization time was defined by time-dependent study of the functionalization; it amounts to 25 min for 3,5-FP, 3-FP, 4-AP, and 15 min for 2-FP. Subsequently, post thermal-annealing treatments (95 °C for 3,5-FP, 3-FP, 2FP and 200 °C for 4-AP) for 20 min is performed in order to remove physisorbed pyridines from the surface. The functionalized samples are measured after being cooled down to room temperature. All the reactions were done in a nitrogen-filled glovebox to exclude the effect from O_2 and

H_2O in air.

Device fabrication and electrical characterization. As-exfoliated MoS_2 monolayer were coated with 2 layers of PMMA (Allresist, 600K/ 950K) immediately after exfoliation to avoid air exposure. Top-contact (80 nm Au) field-effect transistors were fabricated by standard E-beam lithography and lift-off in warm acetone in glovebox. All devices were annealed under vacuum at 200°C overnight to remove absorbents. The characterization of device performance was realized by Keithley 2636A under N_2 atmosphere.

Raman spectroscopy. Raman and Photoluminescence spectra were carried out in inert atmosphere (N_2) by Renishaw inVia spectrometer equipped with 532 nm laser in a nitrogen-filled sealed holder (Linkam). Samples were mounted in the glovebox and immediately measured after annealing or after molecule deposition to avoid exposure to contaminant chemicals. The excitation power was kept below 1 mW to avoid local heating damage effects. The wavenumber (energy) resolution was ~1 meV.

AFM measurement. AFM imaging was performed by means of a Bruker Dimension Icon set-up operating in air, in tapping mode, by using tip model TESPA-V2 (tip stiffness: k=42 N/m).

XPS measurements: Commercial CVD-grown triangle monolayer MoS_2 on Si/SiO_2 (6Carbon Technology (Shenzhen)) was employed to study the surface chemistry of MoS_2, MoS_2/MPc and MoS_2/MPc/fPy. XPS analyses were carried out with a Thermo Scientific K-Alpha X-ray photoelectron spectrometer with a basic chamber pressure of ~10^{-9} mbar and an Al anode as the X-ray source (x-ray radiation of 1486 eV). Spot sizes of 400 μm and pass energies of 200.00 eV for wide energy scans and 10.00-20.00 eV for scans were used.

Photoelectron spectroscopy measurement in air: Commercial CVD-grown triangle monolayer MoS_2 on Si/SiO_2 (6Carbon Technology (Shenzhen)) was employed to measure the experimental work functions of MoS_2, MoS_2/MPc and MoS_2/MPc/fPy by PhotoElectron Yield counter operating in Ambient conditions (PEYA), using a AC-2 Photoelectron Spectrometer (Riken-Keiki Co.). The ambient photoelectron spectroscopy measurements were performed by sampling in each measurement an area of about 4 mm2 (beam size) with an ultraviolet (UV) incident light power of 300 nW with a counting time of 10 seconds per point.

Computational details. All DFT calculations were performed with the projector-augmented wave (PAW) basis set, as implemented in the VASP code. [22] The exchange and correlation effects are treated with the Perdew−Burke−Ernzerhof (PBE) functional,[23] incorporating dipole moment correction along the 'c' axis (Z direction and perpendicular to the MoS_2 surface) and dispersion forces by Grimme correction

(PBE+D2),[24] with a kinetic energy cutoff of 550 eV and using a Monkhorst-Pack mesh of 2×2×1 for the Brillouin zone (BZ) integration. All MPc/fPys were adsorbed on a 10×10 supercell of MoS_2 monolayer with the vacuum space was set to be 25 Å to avoid the interaction with periodic images. Geometries of MoS_2/MPc/fPy heterostructures were fully optimized prior to calculation of work functions. Work function (φ) of heterostructures is calculated as difference of Fermi energy (E_f) and the electrostatic potential at vacuum level (E_p). Fermi level (E_f) is set to the energy of valence band maximum for MoS_2/ZnPc/fPys and for MoS_2/CoPc/fPys, which are open shell systems, E_f is set to the maximum energy of the valence band with doubly occupied electrons ignoring the energy state of the unpaired electron localized on Co.

AUTHOR INFORMATION

PS and YW conceived and coordinated the work. YW worked on sample preparation, device fabrication, optical and electrical characterization. YW analysed the data. SMG & AS did the modelling work, under the supervision of DB. YW and PS wrote the paper with all the authors contributing to the discussion and preparation of the manuscript.

ACKNOWLEDGEMENTS

Device fabrication was carried out in part at the nanotechnology facility eFab (IPCMS, Strasbourg). The authors are thankful to H. Majjad, R. Bernard and S. Siegwald for assistance with microfabrication, as well as Mircea Rastei for the help with the AFM measurements. We acknowledge funding from European Commission through the ERC

project SUPRA2DMAT (GA-833707), the Graphene Flagship Core 2 project (GA-785219), the Agence Nationale de la Recherche through the Labex projects CSC (ANR-10-LABX-0026 CSC) and NIE (ANR-11-LABX-0058 NIE) within the Investissement d'Avenir program (ANR-10-120 IDEX-0002-02), the International Center for Frontier Research in Chemistry (icFRC). The work in Mons is supported by the Belgian National Fund for Scientific Research (FRS-FNRS), within FNRS-PDR-TOREADOR project. Computational resources were provided by the Consortium des Équipements de Calcul Intensif (CÉCI) funded by F.R.S.-FNRS under Grant 2.5020.11. DB is FNRS Research Director.

REFERENCES

[1] a) K. F. Mak, K. L. He, C. Lee, G. H. Lee, J. Hone, T. F. Heinz, J. Shan, *Nat. Mater.* **2013**, *12*, 207; b) Y. D. Zhao, K. Xu, F. Pan, C. J. Zhou, F. C. Zhou, Y. Chai, *Adv. Funct. Mater.* **2017**, *27*, 1603484; c) M. Chhowalla, H. S. Shin, G. Eda, L. J. Li, K. P. Loh, H. Zhang, *Nat. Chem.* **2013**, *5*, 263; d) S. Manzeli, D. Ovchinnikov, D. Pasquier, O. V. Yazyev, A. Kis, *Nat. Rev. Mater.* **2017**, *2*, 17033.

[2] a) B. Radisavljevic, A. Radenovic, J. Brivio, V. Giacometti, A. Kis, *Nat. Nanotechnol.* **2011**, *6*, 147; b) Q. H. Wang, K. Kalantar-Zadeh, A. Kis, J. N. Coleman, M. S. Strano, *Nat. Nanotechnol.* **2012**, *7*, 699; c) S.-L. Li, K. Tsukagoshi, E. Orgiu, P. Samorì, *Chem. Soc. Rev.* **2016**, *45*, 118.

[3] a) L. Britnell, R. M. Ribeiro, A. Eckmann, R. Jalil, B. D. Belle, A. Mishchenko, Y. J. Kim, R. V. Gorbachev, T. Georgiou, S. V. Morozov, A. N. Grigorenko, A. K. Geim, C. Casiraghi, A. H. Castro Neto, K. S. Novoselov, *Science* **2013**, *340*, 1311; b) A. K. Geim, I. V. Grigorieva, *Nature* **2013**, *499*, 419; c) D. Jariwala, V. K. Sangwan, L. J. Lauhon, T. J. Marks, M. C. Hersam, *ACS Nano* **2014**, *8*, 1102; d) X. Wang, F. Xia, *Nat. Mater.* **2015**, *14*, 264; e) D. Jariwala, T. J. Marks, M. C. Hersam, *Nat. Mater.* **2017**, *16*, 170.

[4] a) S. Bertolazzi, M. Gobbi, Y. Zhao, C. Backes, P. Samorì, *Chem. Soc. Rev.* **2018**, *47*, 6845; b) M. Gobbi, E. Orgiu, P. Samorì, *Adv. Mater.* **2018**, *30*, 1706103; c) P. D. Zhao, D. Kiriya, A. Azcatl, C. X. Zhang, M. Tosun, Y. S. Liu, M. Hettick, J. S. Kang, S. McDonnell, K. C. Santosh, J. H. Guo, K. Cho, R. M. Wallace, A. Javey, *ACS Nano* **2014**, *8*, 10808; d) L. Yang, K. Majumdar, H. Liu, Y. Du, H. Wu, M. Hatzistergos, P. Hung, R. Tieckelmann, W. Tsai, C. Hobbs, *Nano Lett.* **2014**, *14*, 6275; e) A. Tarasov, S. Zhang, M. Y. Tsai, P. M. Campbell, S. Graham, S. Barlow, S. R. Marder, E. M.

Vogel, *Adv. Mater.* **2015**, *27*, 1175; f) Y. Wang, A. Slassi, J. Cornil, D. Beljonne, P. Samorì, *Small* **2019**, *15*, 1903432.
[5] a) S. Bertolazzi, S. Bonacchi, G. J. Nan, A. Pershin, D. Beljonne, P. Samorì, *Adv. Mater.* **2017**, *29*, 1606760; b) S. McDonnell, R. Addou, C. Buie, R. M. Wallace, C. L. Hinkle, *ACS Nano* **2014**, *8*, 2880.
[6] a) S. Mouri, Y. Miyauchi, K. Matsuda, *Nano Lett.* **2013**, *13*, 5944; b) S.-H. Jo, D.-H. Kang, J. Shim, J. Jeon, M. H. Jeon, G. Yoo, J. Kim, J. Lee, G. Y. Yeom, S. Lee, H.-Y. Yu, C. Choi, J.-H. Park, *Adv. Mater.* **2016**, *28*, 4824; c) M.-A. Stoeckel, M. Gobbi, T. Leydecker, Y. Wang, M. Eredia, S. Bonacchi, R. Verucchi, M. Timpel, M. V. Nardi, E. Orgiu, P. Samorì, *ACS Nano* **2019**, *13*, 11613.
[7] a) R. Bonnett, *Chem. Soc. Rev.* **1995**, *24*, 19; b) N. B. McKeown, *Phthalocyanine materials: synthesis, structure and function*, Cambridge University Press, **1998**; c) A. B. Sorokin, *Chem. Rev.* **2013**, *113*, 8152; d) A. L. Thomas, *Phthalocyanine research and applications*, CRC Press, **1990**.
[8] J. Choi, H. Zhang, J. H. Choi, *ACS Nano* **2016**, *10*, 1671.
[9] C. J. Benjamin, S. Zhang, Z. Chen, *Nanoscale* **2018**, *10*, 5148.
[10] S. H. Amsterdam, T. K. Stanev, Q. Zhou, A. J.-T. Lou, H. Bergeron, P. Darancet, M. C. Hersam, N. P. Stern, T. J. Marks, *ACS Nano* **2019**, *13*, 4183.
[11] a) Y. Huang, F. Zhuge, J. Hou, L. Lv, P. Luo, N. Zhou, L. Gan, T. Zhai, *ACS Nano* **2018**, *12*, 4062; b) J. Pak, J. Jang, K. Cho, T.-Y. Kim, J.-K. Kim, Y. Song, W.-K. Hong, M. Min, H. Lee, T. Lee, *Nanoscale* **2015**, *7*, 18780.
[12] M.-S. Liao, S. Scheiner, *J. Chem. Phys.* **2001**, *114*, 9780.
[13] B. Przybył, J. Janczak, *Dyes Pigments* **2015**, *118*, 102.
[14] a) Y. Naitoh, T. Matsumoto, K.-i. Sugiura, Y. Sakata, T. Kawai, *Surf. Sci.* **2001**, *487*, L534; b) R. Strohmaier, C. Ludwig, J. Petersen, B. Gompf, W. Eisenmenger, *J. Vac. Sci. Technol. B* **1996**, *14*, 1079; c) P. Choudhury, L. Ravavarapu, R. Dekle, S. Chowdhury, *J. Phys. Chem. C* **2017**, *121*, 2959.
[15] Y. Zhao, S. Bertolazzi, P. Samorì, *ACS Nano* **2019**, *13*, 4814.
[16] T. R. Kafle, B. Kattel, P. Yao, P. Zereshki, H. Zhao, W.-L. Chan, *J. Am. Chem. Soc.* **2019**.
[17] D. R. Tackley, G. Dent, W. E. Smith, *Phys. Chem. Chem. Phys.* **2000**, *2*, 3949.
[18] a) L. Chen, Y. Gao, Y. Cheng, H. Li, Z. Wang, Z. Li, R.-Q. Zhang, *Nanoscale* **2016**, *8*, 4086; b) P. M. Wojciechowski, W. Zierkiewicz, D. Michalska, P. Hobza, *J. Chem. Phys.* **2003**, *118*, 10900.
[19] Y. Li, C.-Y. Xu, P. Hu, L. Zhen, *ACS Nano* **2013**, *7*, 7795.
[20] M. Gobbi, S. Bonacchi, J. X. Lian, A. Vercouter, S. Bertolazzi, B. Zyska, M. Timpel, R. Tatti, Y. Olivier, S. Hecht, M. V. Nardi, D. Beljonne, E. Orgiu, P. Samorì, *Nat. Comm.* **2018**, *9*, 2661.
[21] a) Y. Wang, A. Slassi, M.-A. Stoeckel, S. Bertolazzi, J. Cornil, D. Beljonne, P. Samorì, *J. Phys. Chem. Lett.* **2019**; b) H. V. Han, A. Y. Lu, L. S. Lu, J. K. Huang, H. Li, C. L. Hsu, Y. C. Lin, M. H. Chiu, K. Suenaga, C. W. Chu, H. C. Kuo, W. H. Chang, L. J. Li, Y. Shi, *ACS Nano* **2016**, *10*, 1454; c) K. F. Mak, K. He, C. Lee, G. H. Lee, J. Hone, T. F. Heinz, J. Shan, *Nat. Mater.* **2013**, *12*, 207; d) W. Su, H. Dou, D. Huo, N. Dai, L. Yang, *Chem. Phys. Lett.* **2015**, *635*, 40.
[22] a) G. Kresse, J. Furthmüller, *Phys. Rev. B* **1996**, *54*, 11169; b) G. Kresse, M. Marsman, J. Furthmüller, VASP, 2012.
[23] J. P. Perdew, K. Burke, M. Ernzerhof, *Phys. Rev. Lett.* **1996**, *77*, 3865.
[24] S. Grimme, *J. Comput. Chem.* **2006**, *27*, 1787.